Calculation of spontaneous emission and gain spectra for quantum cascade lasers

2000 J. Phys.: Condens. Matter 12 1907

(http://iopscience.iop.org/0953-8984/12/8/332)

J. Phys.: Condens. Matter **12** (2000) 1907–1914. Printed in the UK PII: S0953-8984(00)08844-5

Calculation of spontaneous emission and gain spectra for quantum cascade lasers

Q K Yang and A Z Li

State Key Laboratory of Functional Materials for Informatics, Shanghai Institute of Metallurgy, Chinese Academy of Sciences, Shanghai 200050, People's Republic of China

Received 20 October 1999

Abstract. In this paper, a quantum cascade laser has been treated as a three-level system, and the calculation of the spontaneous emission and gain spectra has been given. In the calculation, the conduction band nonparabolicity and the injection and exit of electrons have been considered. Results have shown that with increasing injection current, the spontaneous emission peak blue shifts, and the peak intensity increases near linearly with current. With increasing temperatures, the broadening of the spontaneous emission spectra has been attributed to the electron–optical phonon interactions. The peak gain of the stimulated emission has been shown to be determined mainly by the subband lifespans. We have pointed out that it is essential to obtain a long lifespan for the second excited state and short lifespan for the first excited state in order to obtain efficient population inversion and high peak gain for quantum cascade lasers.

1. Introduction

Quantum cascade (QC) lasers based on GaInAs/AlInAs heterostructures have been shown to be new light sources working in the important infrared atmospheric window [1–5], which used to be only accessible to cryogenic lead-salt lasers [6]. Compared with conventional semiconductor lasers based on the recombination of electrons in the conduction band and holes in the valence band, QC lasers need only electrons to transit between conduction subbands created by quantum confinement, i.e. QC lasers are unipolar semiconductor lasers.

Since their first demonstration [1], QC lasers have been expected to exhibit the following features as a characteristic of the intersubband transitions: (1) the lasers should be able to operate in the wavelength region from a few micrometres to submillimetre, because the emission wavelength is completely determined by the thickness of layers and not the bandgap of the active materials in the case of conventional interband semiconductor lasers; (2) the gain spectra should be narrow and symmetric; (3) a weak temperature dependence of the threshold current should be available. Up to now, QC lasers based on GaInAs/AlInAs heterostructures working at the wavelength from 3.4 μm to 17 μm have been demonstrated [7–9], while much less effort has been spent on the gain spectra of QC lasers. Gelmont *et al* and Gorfinkel *et al* reported their calculation of gain spectra for QC lasers based on an infinite-well model and have achieved reasonable results [10, 11]. In this paper, it is our purpose to calculate the spontaneous emission and gain spectra for practical QC lasers.

Figure 1 is a typical conduction band diagram of a portion of QC lasers working at $\lambda \sim 5$ μm. In figure 1, A.R. denotes the active region and the black areas are minibands in the graded-gap superlattice, i.e., injection/relaxation region. Between the minibands are minigaps where electrons are not allowed to exist. In the active region, electrons transit from

0953-8984/00/081907+08$30.00

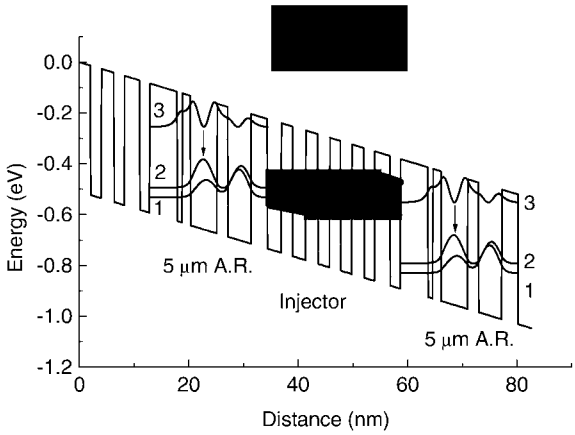

Figure 1. Schematic conduction band diagram of a portion of the active region of a typical $\lambda \sim 5\,\mu$m structure. The shaded areas indicate the allowed minibands of electrons in the injector region.

the $n = 3$ state to the $n = 2$ state and emit photons. The $n = 2$ state is promptly emptied by the resonant scattering between the $n = 2$ state and $n = 1$ state with the help of optical phonons. ($\tau_{21} \sim 0.5$ ps). Population inversion can be achieved between the $n = 3$ state and the $n = 2$ state because transition from the $n = 3$ state to the $n = 2$ state involves large momentum transfer ($\tau_{32} \sim 1.5$ ps).

2. Methods

As has been pointed out by many authors, energy band nonparabolicity is a factor that should not be ignored in semiconductor lasers [10–13]. In the present work, conduction band nonparabolicity has been characterized with an energy-dependent effective mass. After Sirtori *et al* [12], we start from the envelope-function Hamiltonian in the Kane approximation. Considering the spin degeneracy and the decoupling of the heavy-hole state from the original Hamiltonian, and adopting a proper unitary transformation to the reduced Hamiltonian, one obtains

$$m(E, z) = m_0 \frac{E - E_v(z)}{E_p} \tag{1}$$

which can be used to characterize the conduction band nonparabolicity. In equation (1) m_0 is the static electron mass, z is the growth direction, $E_v(z)$ is the band edge energy for the effective valence band which is the result of the unitary transformation. $E_v = (2E_{th} + E_{so})/3$, where lh and so label light-hole and split-off position dependent band edges, and E_p is the Kane energy. In this paper, E is measured from the bottom of the GaInAs conduction band, E_v is taken as 0.92 eV and 1.23 eV for the GaInAs well and AlInAs barrier, respectively, and E_p is taken as 21.9 eV. Substituting equation (1) into the expression

$$E = E_n + \frac{\hbar^2 k_\parallel^2}{2m(E)} \tag{2}$$

under the envelope-function approximation, where E_n is the quantized energy as a result of the confinement in the z direction, $k_\parallel$ is the in-plane wavevector, $\hbar$ is the reduced Planck constant,

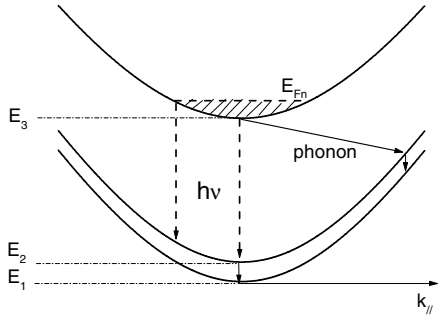

Figure 2. The E–k relationship for the subbands with conduction band nonparabolicity being considered. The dashed arrows are associated with photon emission, while the solid arrows are associated with phonon emission.

one can obtain a quadratic equation in E. Solving the equation one obtains

$$E = E_n + \frac{E_v - E_n + \sqrt{(E_v - E_n)^2 + 2E_p\hbar^2k_\parallel^2/m_0}}{2} \tag{3}$$

which is the E–k relationship under this approximation as schematically shown in figure 2. Many calculated results after this approximation have been shown to be in excellent agreement with experimental ones [12–14].

The transition rate for the emission of a photon if an electron is initially at state E_b is given by Fermi's golden rule and can be derived using the time-dependent perturbation theory as

$$W_{ems} = \frac{2\pi}{\hbar}|\langle \mathrm{a}|H'|\mathrm{b}\rangle|^2\delta(E_a - E_b + \hbar\omega) \tag{4}$$

where E_a is the final state, ω is the photon frequency and H' is the perturbation Hamiltonian. The total transition rate per unit volume (s^{-1} cm^{-1}), taking into account the probability that state b and state a are partly occupied, is

$$R_{b\to a} = \frac{2}{V}\sum_{k_a}\sum_{k_b}\frac{2\pi}{\hbar}|H'_{ab}|^2\delta(E_a - E_b + \hbar\omega)\,f_b(1 - f_a). \tag{5}$$

In terms of the dipole moment, the spontaneous emission lineshape can be written as

$$I(\hbar\omega) \sim \frac{\pi\omega}{n_r c\varepsilon_0}\frac{2}{V}\sum_{k_a}\sum_{k_b}\frac{2\pi}{\hbar}|\hat{e}\cdot\bar{\mu}_{ab}|^2\delta(E_a - E_b + \hbar\omega)\,f_b(1 - f_a) \tag{6}$$

where n_r is the refractive index, ε_0 is the vacuum dielectricity, μ_{ab} is the electric dipole moment, c is the speed of light in free space and $\hat{e}$ is the unit vector for electric field.

When the scattering relaxation is included, the delta function may be replaced by a Lorentzian function with a linewidth Γ:

$$\delta(E_a - E_b + \hbar\omega) \to \frac{\Gamma/(2\pi)}{(E_a - E_b + \hbar\omega)^2 + (\Gamma/2)^2}. \tag{7}$$

Because of the selection rule, only TM modes exist for intersubband transitions in the case of QC lasers [15], the two summations in expression (6) can be reduced to one and

$$I(\hbar\omega) \sim \frac{\pi\omega}{n_r c\varepsilon_0}\frac{2}{V}\sum_{k_{ta}}\frac{|\mu_{ab}|^2(\Gamma/2\pi)}{(E_a - E_b + \hbar\omega)^2 + (\Gamma/2)^2}\,f_b(1 - f_a) \tag{8}$$

where k_t is the in-plane wavevector, and $|a\rangle$, $|b\rangle$ are envelope functions for final ($n = 2$ in figure 1) and initial ($n = 3$) subband states, respectively.

The summation in (8) can be replaced by an integral

$$\frac{2}{V}\sum_{k_t} = \frac{1}{2\pi_2 L_p}\int \mathrm{d}^2 k_t = \frac{m_e^*}{\pi\hbar^2 L_p}\int \mathrm{d}E_t \tag{9}$$

where L_p is the thickness of one period in QC lasers, E_t is the in-plane energy.

The distribution functions f_b and f_a are determined by their respective quasi-Fermi energy levels and the Fermi–Dirac distribution for electrons,

$$f_a = \frac{1}{1+\exp((E_a + E_t - F_a)/k_B T)} \tag{10a}$$

$$f_b = \frac{1}{1+\exp((E_b + E_t - F_b)/k_B T)} \tag{10b}$$

where F_a and F_b are quasi-Fermi levels for a and b states, respectively, k_B is the Boltzmann constant and T is temperature. The E_a and E_b are quantized energies which can be readily obtained by solving the Schrödinger equation [13, 14].

In the case of QC lasers where electrons are only injected into the $n = 3$ state, $F_3(F_b)$ is determined to a large extent by the injection current, while $F_2(F_a)$ can be approximately obtained by taking into account of the doping concentration and the electrons jumping from the $n = 3$ state to the $n = 2$ state.

Gain in lasers can be expressed as

$$g(\hbar\omega) = \frac{R_{b\to a} - R_{a\to b}}{(S/\hbar\omega)} = \left(\frac{\omega}{n_r c\varepsilon_0}\right)\frac{m_e^*}{\pi\hbar^2 L_p} \times \int_0^\infty \mathrm{d}E_t \frac{|\mu_{23}|^2(\Gamma/2\pi)}{(E_2 - E_3 + \hbar\omega^2) + (\Gamma/2)^2}[f_3(E) - f_2(E)] \tag{11}$$

where S represents area.

3. Results and discussion

3.1. Spontaneous emission spectra

The injection current density j can be estimated by

$$j = nev \tag{12}$$

where e is the unit charge, n is the electron density, v is the transportation velocity of electrons,

$$v = \frac{L_p}{\tau} \tag{13}$$

where τ is the time for an electron to pass through one period of a QC laser,

$$\tau = \tau_{32} + \tau_{21} + \tau_1 + \tau_{gs} \tag{14}$$

where τ_{32}, τ_{21} are transition times of electrons from the $n = 3$ to $n = 2$ state, and from the $n = 2$ to $n = 1$ state, respectively, τ_1 is the tunnelling time to the empty $n = 1$ state (see figure 1), and τ_{gs} is the time for electrons to tunnel across the graded-gap superlattice region.

Substituting (13) into (12) one obtains

$$j = n_{2D} e\frac{1}{\tau} \tag{15}$$

where n_{2D} is the injection sheet density.

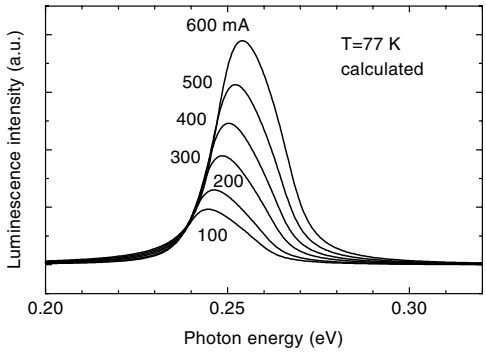

Figure 3. The calculated EL lineshape for the QC laser shown in figure 1 at $T = 77$ K and at different injection currents. The threshold current has been assumed to be 1.5 A. The blue shift of the peak with increasing current is an effect associated with the Stark effect of intersubband transition.

When the injection current is small, electric luminescence (EL) can be obtained as a result of spontaneous emission. At low temperatures, the $n = 2$ state can be regarded as empty because of the short lifespan τ_{21}, the small injection current density and the consequent small number of injected electrons.

Because F_b is mainly determined by the injection current density, two features can be expected for spontaneous emission spectra with increasing injection densities: (1) Blue shift of the EL peak as a result of the increasing F_b and the increasing bias, since the V–I curve exhibits a linear behaviour below threshold current. (2) Higher peak intensity because more electrons are injected into the $n = 3$ state.

Figure 3 is the calculated EL lineshape taking the QC laser shown in figure 1 as an example at $T = 77$ K and at different injection currents (the threshold current has been assumed to be 1.5 A). The blue shift of the peak with increasing current is an effect associated with the Stark effect of intersubband transition. The peak intensity has been shown to increase nearly linearly with the injection current since at low temperature, the quasi-Fermi level almost increases linearly with injection current density.

At higher temperatures, the broadening of the linewidth and the backfilling of electrons from the ground state in the injection/relaxation region to the $n = 2$ state should be considered [16]. As has been pointed out in our previous works [17], interface fluctuations are inevitable even in molecular-beam-epitaxy-grown device quality materials. Taking into account the electron–LO phonon interaction, like the photoluminescence linewidth [18], the EL linewidth can be expressed as

$$\Gamma = \Gamma_i + \Gamma_c \left[\exp\left(\frac{\hbar\omega_{LO}}{k_B T} \right) - 1 \right]^{-1} \tag{16}$$

where the temperature-independent term Γ_i is composed of the intrinsic linewidth, linewidth broadening caused by alloy scattering and linewidth broadening caused by interface roughness. The second term in equation (16) represents the electron–LO phonon interaction. Γ_i and Γ_c are empirically determined to be 15 meV and 18 meV respectively for the exemplified $\lambda \sim 5$ μm QC laser. The calculated spontaneous emission lineshapes for this structure at $T = 10$ K, 100 K, 200 K and 300 K are shown in figure 4. In the calculation, we have considered the thermal backfilling, and the shrinkage of the conduction band offset, i.e. the well depth, with increasing temperatures and the consequent energy shift.

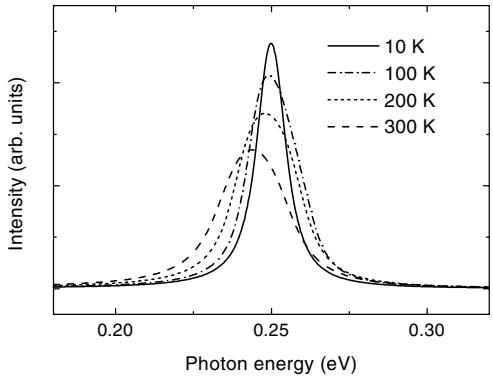

Figure 4. The calculated spontaneous emission lineshapes at $T = 10$ K, 100 K, 200 K and 300 K.

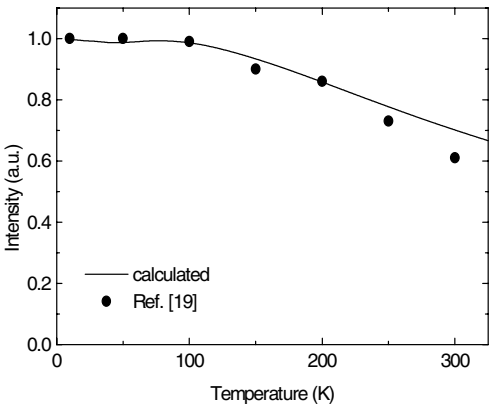

Figure 5. The calculated EL integral intensity as a function of temperature (solid line). The solid circles are experimental results after [19].

As is well known, one of the key features for photoluminescence (PL) used to characterize the interband transitions is the thermal quenching of the integral intensity. However, from figure 4, one can easily see that there is only a slight drop of intensity with increasing temperature, as plotted in figure 5. The result is in good agreement with experiments and can be attributed to the selected injection of electrons into the $n = 3$ state [19].

3.2. Gain spectra

When the injection current density is large enough to be above the threshold current density, the $n = 2$ state cannot be assumed to be empty any more. The empty time namely τ_{21} should be taken into account.

For stimulated emission, dynamic equilibrium is achieved. Focusing on the $n = 2$ state in figure 1, there should be

$$\mathrm{d}n_2 = A_{32}n_3\,\mathrm{d}t - A_{21}n_2\,\mathrm{d}t \tag{17}$$

where the first term of the right side is the incoming electrons from the $n = 3$ state in time

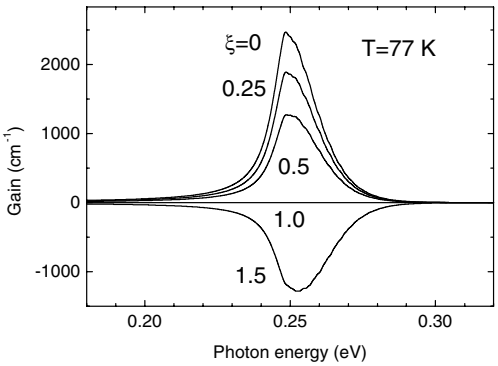

Figure 6. Calculated gain spectra of the QC laser for different population-inversion parameter $\xi = n_2/n_3 = \tau_{21}/\tau_{32}$. The population inversion condition $\tau_{21} \leqslant \tau_{32}$ can be readily obtained from this figure.

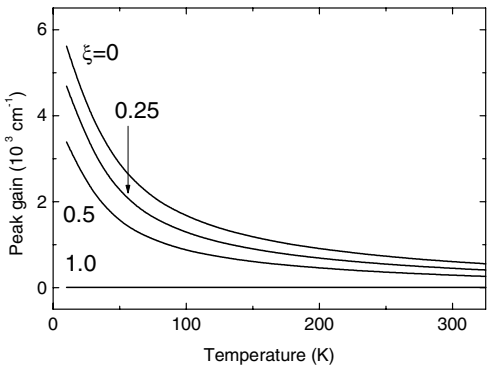

Figure 7. The calculated peak gain as a function of temperature.

interval dt, and the second term is the outgoing electrons to the $n = 1$ state in time dt. A is Einstein's coefficient, n is the number of electrons in a certain state.

For the dynamic equilibrium condition

$$\frac{\mathrm{d}n_2}{\mathrm{d}t} = 0 \tag{18}$$

one obtains

$$\frac{n_2}{n_3} = \frac{A_{32}}{A_{21}} = \frac{\tau_{21}}{\tau_{32}}. \tag{19}$$

For different population-inversion parameter $\xi = n_2/n_3 = \tau_{21}/\tau_{32}$, the gain spectra of the QC laser shown in figure 1 are calculated and shown in figure 6. In practical QC lasers, mirror loss and waveguide loss should be considered, and the gain spectra will be vertically shifted by a few tens of wavenumbers to discount the loss. The population inversion condition $\tau_{21} \leqslant \tau_{32}$ can be readily obtained from figure 6.

Figure 7 is the calculated peak gain as a function of temperature for the same exemplified structure. The peak gain is shown to decrease with increasing temperatures, and with increasing population-inversion parameter ξ. It should be noted that peak in gain occurs at different wavelengths for different temperatures; linear shift to longer wavelengths with increasing

temperatures is expected within a rather large range of temperatures. In this way tunable QC lasers have been achieved by tuning the heat-sink temperature [20, 21]. It is obvious that all of the above calculations can be easily adapted to QC lasers working at other wavelengths.

4. Conclusion

In summary, by taking into account the conduction band nonparabolicity, and injection and exit of electrons in and out of the active region, we have calculated the spontaneous emission and gain spectra for quantum cascade lasers. A practical $\lambda \sim 5$ μm quantum cascade laser is taken as an example. The influence of temperature and population inversion parameter on the spontaneous emission and gain spectra has been discussed.

Acknowledgments

The authors would like to thank Dr C Gmachl for helpful discussions. This work is supported in part by the Chinese Academy of Sciences under contract No KJ951-B1-706-01.

References

[1] Faist J, Capasso F, Sivco D L, Sirtori C, Hutchinson A L and Cho A Y 1994 *Science* **264** 553
[2] Scamarcio G, Capasso F, Sirtori C, Faist J, Hutchinson A L, Sivco D L and Cho A Y 1997 *Science* **276** 5313
[3] Faist J, Capasso F, Sirtori C, Sivco D L, Hutchinson A L and Cho A Y 1997 *Nature* **387** 777
[4] Gmachl C, Capasso F, Narimanov E E, Nockel J H, Stone A D, Faist J, Sivco D L and Cho A Y 1998 *Science* **280** 1556
[5] Tredicucci A, Gmachl C, Capasso F, Sivco D L, Hutchinson A L and Cho A Y 1998 *Nature* **396** 350
[6] Tacke M 1995 *Infrared Phys. Technol.* **36** 447
[7] Capasso F, Faist J, Sirtori C and Cho A Y 1997 *Solid State Commun.* **102** 231
[8] Faist J, Capasso F, Sivco D L, Hutchinson A L and Cho A Y 1998 *Appl. Phys. Lett.* **72** 680
[9] Tredicucci A, Gmachl C, Capasso F, Sivco D L, Hutchinson A L and Cho A Y 1997 *Appl. Phys. Lett.* **71** 638
[10] Gelmont B, Gorfinkel V and Luryi S 1996 *Appl. Phys. Lett.* **68** 2171
[11] Gorfinkel V B, Luryi S and Gelmont B 1996 *IEEE J. Quantum Electron.* **32** 1995
[12] Sirtori C, Capasso F, Faist J and Scandolo S 1994 *Phys. Rev.* B **50** 8663
[13] Yang Q K and Li A Z 1999 *Physica* E **4** 239
[14] Yang Q K and Li A Z 1999 *Chin. Phys. Lett.* **16** 443
[15] Sirtori C, Capasso F, Faist J, Sivco D L, Hutchinson A L and Cho A Y 1995 *Appl. Phys. Lett.* **66** 4
[16] Faist J, Capasso F, Sivco D L, Hutchinson A L, Sirtori C, Chu S N G and Cho A Y 1994 *Appl. Phys. Lett.* **65** 2901
[17] Yang Q K, Chen J X and Li A Z 1999 *J. Cryst. Growth* at press
[18] Yang Q K, Chen J X and Li A Z 1998 *J. Cryst. Growth* **194** 31
[19] Faist J, Capasso F, Sirtori C, Sivco D L, Baillargeon J N, Hutchinson A L and Cho A Y 1996 *Appl. Phys. Lett.* **68** 3680
[20] Gmachl C, Capasso F, Faist J, Hutchinson A L, Tredicucci A, Sivco D L, Baillargeon J N, Chu S N G and Cho A Y 1998 *Appl. Phys. Lett.* **72** 1430
[21] Gmachl C, Tredicucci A, Capasso F, Hutchinson A L, Sivco D L, Baillargeon J N and Cho A Y 1998 *Appl. Phys. Lett.* **72** 3130